ELSEVIER

Journal of Nuclear Materials 283–287 (2000) 259–262

journal of nuclear materials

www.elsevier.nl/locate/jnucmat

Section 3. Microstructures and irradiated materials

Microstructural changes in a low-activation Fe–Cr–Mn alloy irradiated with 92 MeV Ar ions at 450°C

Chonghong Zhang [a], Keqin Chen [a,*], Yinshu Wang [a], Jiguang Sun [b], Benfu Hu [c], Yunfan Jin [a], Mingdong Hou [a], Changlong Liu [a], Youmei Sun [a], Jin Han [a], Chaoqing Chen [b]

[a] *Institute of Modern Physics, Chinese Academy of Sciences, P.O. Box 31, Lanzhou 730000, People's Republic of China*
[b] *General Research Institute for Nonferrous Metals, Beijing 100088, People's Republic of China*
[c] *University of Science and Technology Beijing, Beijing 100083, People's Republic of China*

Abstract

In this work, a solution-annealed specimen of a low-activation Fe–Cr–Mn alloy was irradiated with 92 MeV Ar ions at 450°C to a dose of 1.7×10^{21} m^{-2} which was expected to produce a peak displacement damage of 90 dpa. After irradiation, damage microstructure was investigated from the cross-sectional specimens using a transmission electron microscope. High number density cavities were observed in the peak dose region. Size of cavities was the largest at the peak displacement damage. Formation of α-phase was found at a grain boundary in the peak dose region. Well-dispersed carbide particles was found in the matrix. The carbide/matrix interfaces supplied favorable site for growth of large cavities, whereas only small cavities were found inside the particles.

1. Introduction

In the past decade, low-activation materials are considered for fusion reactor applications because of their low-induced radioactivity and associated environmental and safety concerns. The austenitic Fe–Cr–Mn alloys produce much lower induced radioactivity than Fe–Cr–Ni alloys, and addition of oversize solutes such as W and V into Fe–Cr–Mn alloys is known to improve the resistance to void-swelling and stabilize γ-phase [1]. The alloys were designed generally for use below 450°C. Swelling and embrittlement are the main concerns for the nuclear reactor applications of these alloys. To investigate defect production, void swelling and solute segregation at grain boundaries in the alloys, some studies have been performed with electron beam or electron/helium dual beam irradiation in high-voltage electron microscope (HVEM) [1,2]. In the present work, microstructural evolution in a low-activation Fe–Cr–Mn alloy was studied after irradiation with high-energy Ar ions to a high dose at 450°C.

2. Experimental procedure

The composition of the studied austenitic Fe–Cr–Mn alloy is listed in Table 1. The alloy was melted in a vacuum of 10^{-2} Pa, and had a final solution-annealing treatment at 1050°C for 1 h in a vacuum of 6×10^{-6} Pa. A polished sheet specimen of 10 mm × 5 mm × 0.2 mm dimension was irradiated with 92 MeV ^{18}Ar ions in a chamber connected to a 1.7 m cyclotron in the National Laboratory of Heavy-ion Accelerator in Lanzhou. Ion beam intensity was measured with a sandwich-type apparatus of aluminum foils, which was placed in front of the target holder. The specimen temperature was maintained at 450 ± 20°C during irradiation. The irradiation parameters are described in Table 2. The employed peak damage dose and argon concentration were 90 dpa (displacement per atom) and ~4 at.%, respectively, according to TRIM-92 code (Fig. 1).

* Corresponding author. Tel.: +86-931 885 4867; fax: +86-931 888 1100.
E-mail address: hiam@ns.lzb.ac.cn (K. Chen).

0022-3115/00/$ - see front matter
PII: S0022-3115(00)00207-5

Table 1
Composition of Fe–Cr–Mn alloy used in present study (wt%)

C	N	Ni	W	V	Mn	Cr	Fe
0.3	0.1	0.1	2	2	15	15	Bal.

Table 2
Parameters of irradiation with 92 MeV Ar ions

Specimen T (°C)	Dose (ions/m^2)	Time (h)	dpa (peak)	C_{Ar} (peak, at.%)
450	1.7×10^{21}	~80	90	~4

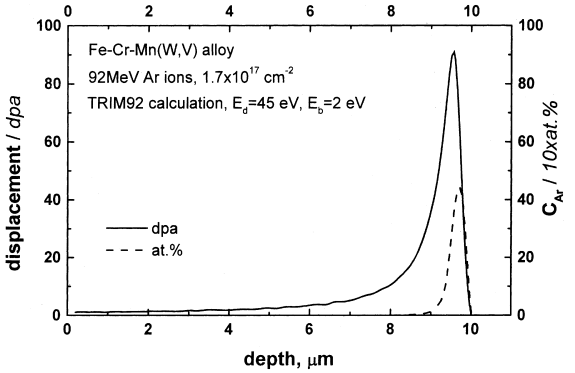

Fig. 1. Depth profiles of displacement damage (dpa) and argon concentration for Fe–Cr–Mn alloy irradiated with 92 MeV ^{18}Ar ions (TRIM-92 code).

After irradiation, specimens were electro-plated with nickel in $NiCl_2/NiSO_4$ acid solution to a thickness of 3 mm, and were cut into cross-sectional foils. The cross-sectional TEM foils were prepared by ion beam milling, and examined by using a JEM-2000FX transmission electron microscope.

3. Results and discussion

3.1. Cavity formation

High number density cavities were observed at the peak dose region spanning a depth from 9 to 10 μm beneath the irradiated surface. A typical cross-sectional micrograph is shown in Fig. 2. The cavity microstructure varies with depth indicating the dependence of cavity nucleation and growth on dpa and Ar concentration. Two different size classes of cavities were clearly observed at the peak damage region, ones with average diameter of ~3 nm, and the other ones with average diameter of ~10 nm, while cavities with intermediate diameter are much fewer (Fig. 3). Similar bi-modal cavity size distribution was observed in other experiments for stainless steels irradiated with heavy ions at intermediate temperatures, when gas atoms (He, O etc.) were implanted before or during heavy-ion irradiation [3–5]. The appearance of the bi-modal size distribution was thought to originate from the difference in gas pressure within cavities, only those cavities with pressure higher than a critical value can effectively trap vacancies and grow into large ones, while others with pressure lower than a critical value cannot grow [6]. This study

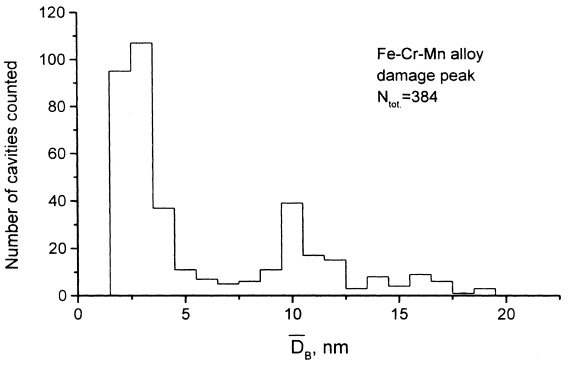

Fig. 3. Distribution of cavities on diameter in the peak dose region.

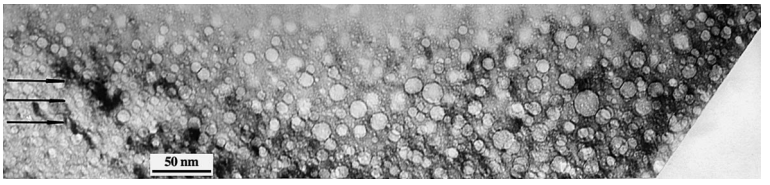

Fig. 2. Typical cross-sectional micrograph of the irradiated peak dose region, the arrows show the incident direction of ions.

indicates that Ar atoms appear to behave like He or O atoms and contribute to the formation of the bi-modal size distribution of cavities.

From the enlarged cross-sectional micrographs, we measured number density and mean effective diameter of cavities as a function of depth along the incident direction of Ar ions. The depth profiles of number density and mean diameter of cavities are shown in Fig. 4(a) and (b) respectively, where the depth '0' represents the shallowest depth where cavities were observed. The depth profiles of two classes of cavities show different dose dependence. The mean diameter of the small size class is weakly dependent on dpa and argon concentration, while that of the large class has strong dependence on dose. Large cavities were developed and get their maximum size at the peak displacement damage region indicating that the high vacancy supersaturation at the peak damage region is responsible for the faster cavity growth.

It is interesting to compare the data of cavities obtained in the present work with those obtained in the similar Fe–Cr–Mn alloys irradiated with electron beam or electron/helium dual beam in high-voltage electron microscopes (HVEM) [1,2]. The data of cavities and corresponding irradiation conditions are compiled in Table 3. A large difference in cavity structures was found in different irradiation conditions. For the irradiation with Ar ions, the number density of cavities is two to three orders of magnitude higher while the cavity size is much smaller than those from the HVEM irradiation experiment indicating that the very high concentration of implanted argon (up to ~4 at.%) is responsible for the enhanced nucleation of cavities and the suppressed growth of cavities. In this case, the cavities are believed to be argon bubbles rather than voids.

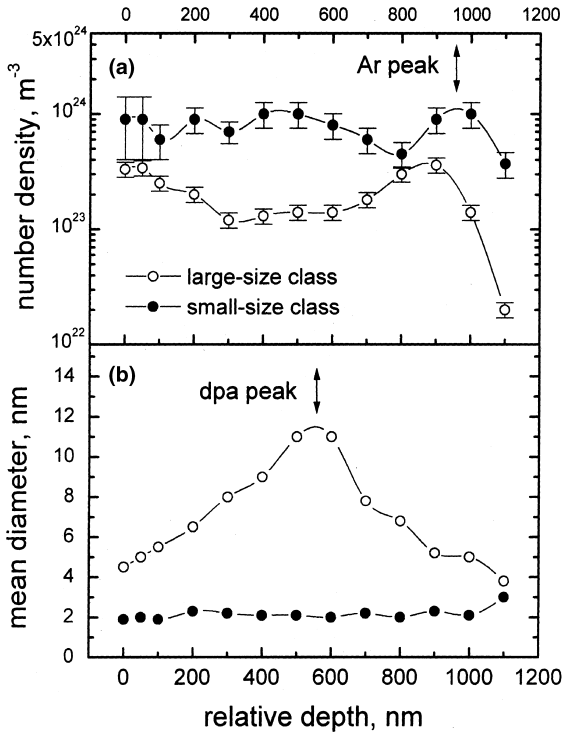

Fig. 4. Depth profile of :(a) number density; (b) mean diameter of cavities in the Fe–Cr–Mn alloy specimen irradiated with 92 MeV Ar ions, where the depth '0' represents the shallowest depth of the visible cavities.

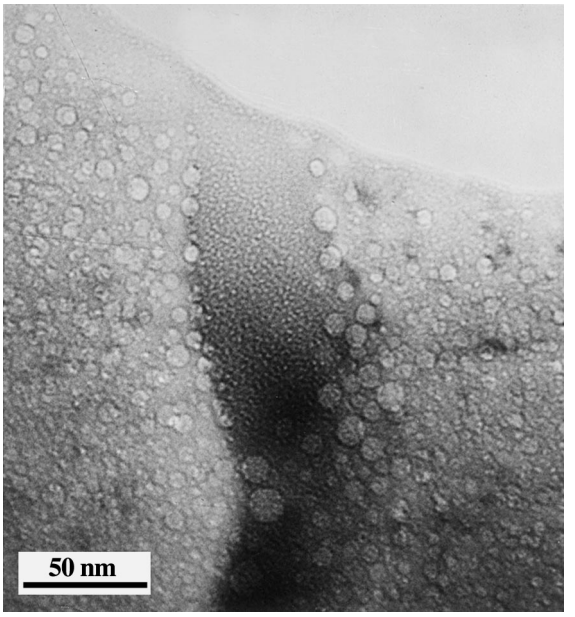

Fig. 5. α-phase at grain boundaries in the peak dose region.

Table 3
Different irradiation conditions of Fe–Cr–Mn alloys and microstructural data of cavities obtained

Irradiation experiment	T (°C)	Dose (dpa)	Dose (appm gas)	Dose rate (dpa/s)	Number density (m^{-3})	Mean diameter (nm)
92 MeV Ar ion beam	450	90 (max.)	4×10^4 (peak)	$\sim2\times10^{-4}$	3×10^{23} (max.)	~10 (max.)
Electron single beam	450	60	0	2×10^{-3}	3×10^{20}	>100
Electron/helium beam	450	9	180	2×10^{-3}	4×10^{21}	~45

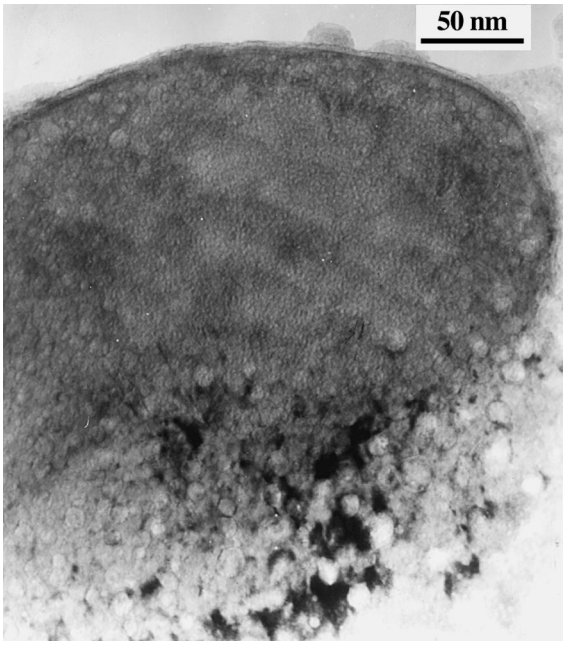

Fig. 6. Typical morphology of carbide particles in the peak dose region.

3.2. Phase instability at grain boundary

The micrograph shown in Fig. 5 gives evidence of the formation of α-phase at grain boundaries in the peak dose region. Large cavities formed at the interfaces between α-phase and the matrix, while much smaller ones were observed within the α-phase. The formation of α-phase at grain boundaries seems to occur only at high dose, since it was not observed in similar alloy irradiated with electron/helium dual beam to 9 dpa [2].

3.3. Carbide particles after irradiation

Due to the addition of W and V to the alloy, dispersed carbide particles with size around 0.5 μm were present in the matrix. The carbide particles were very stable throughout the irradiation, and cavity growth inside the particles was very limited and only very fine cavities or bubbles were observed within them. However, the carbide/matrix interfaces supplied favorable sites for growth of large cavities (Fig. 6).

4. Conclusion

Cavities with high number density were found at the peak dose region in a low-activation Fe–Cr–Mn alloy irradiated with 92 MeV ^{18}Ar ions to 90 dpa at 450°C. A bi-modal size distribution of cavities was found. The size of larger class cavities became the largest at the peak displacement damage region.

Formation of α-phase was observed at grain boundaries in the peak dose region. Very fine cavities or bubbles were found within carbide particles, whereas the carbide/matrix interfaces supplied favorable sites for growth of large cavities.

Acknowledgements

Work is supported by Chinese Fission–Fusion Hybrid Reactor Committee, Chinese Academy of Sciences, and the National Science Foundation of China.

References

[1] H. Benfu, H.Takahashi, in: X. Deng et al. (Eds.), Proceedings of the Third Sino-Japanese Syposium Materials for Advanced Energy System and Fission and Fusion Engineering, Chengdu, November 1995, p. 181.
[2] H. Benfu, H. Kinoshita, H. Takahashi, J. Nucl. Mater. 258–263 (1998) 1708.
[3] R.L. Sindelar, G.L. Kulcinsky, R.A. Dodd, J. Nucl. Mater. 122&123 (1984) 246.
[4] D.J. Mazey, R.S. Nelson, J. Nucl. Mater. 85&86 (1979) 671.
[5] N.H. Packan, J. Nucl. Mater. 103&104 (1981) 1029.
[6] L.K. Mansur, W.A. Coghlan, J. Nucl. Mater. 119 (1983) 1.